atmosphere

MDPI

Article

A Methodological Approach Using ENVI-Met Simulations and Meteorological Data for Assessing Thermal Stress: The Case of Athens (Greece)

Ioannis Koletsis [1,2,*], Katerina Pantavou [1,2,*], Spyridon Lykoudis [3], Areti Tseliou [1,4], Antonis Bezes [2], Ioannis X. Tsiros [1], Konstantinos Lagouvardos [2], Basil E. Psiloglou [2], Dimitra Founda [2] and Vassiliki Kotroni [2]

[1] Laboratory of General and Agricultural Meteorology, Agricultural University of Athens, Iera Odos St. 75, GR 11855 Athens, Greece; tseliou.areti@ac.eap.gr (A.T.); itsiros@aua.gr (I.X.T.)
[2] Institute for Environmental Research and Sustainable Development, National Observatory of Athens, P. Penteli, GR 15236 Athens, Greece; antbezes@noa.gr (A.B.); lagouvar@noa.gr (K.L.); bill@noa.gr (B.E.P.); founda@noa.gr (D.F.); kotroni@noa.gr (V.K.)
[3] Independent Researcher, Lykourgou 235, GR 17576 Athens, Greece; s.lykoudis65@yahoo.com
[4] Laboratory of Technology and Policy of Energy and the Environment, School of Applied Arts and Sustainable Design, Hellenic Open University, Parodos Aristotelous 18, GR 26335 Patra, Greece
* Correspondence: koletsis@noa.gr (I.K.); kpantav@noa.gr (K.P.)

Abstract

Climate change and rising global temperature values lead to a cascade of effects on human health and well-being. Methodologies for assessing thermal conditions and identifying areas with increased thermal stress are important for enhancing the quality of life in urban environments. This study is aimed at developing a methodology that combines high-resolution simulation data with surface meteorological observations for application in urban thermal stress assessment. Eleven urban public sites within the metropolitan area of Athens, Greece (i.e., squares and parks) were simulated using the three-dimensional microclimate model ENVI-met. The model was validated using micrometeorological data from field campaigns conducted in summer, autumn and winter. The validation results confirmed that ENVI-met showed satisfactory performance for further research analysis. Subsequently, Physiologically Equivalent Temperature (PET) and Universal Thermal Climate Index (UTCI) were calculated using data from weather stations operated by the National Observatory of Athens and the Hellenic National Meteorological Service. PET and UTCI were then spatially interpolated using a mixed modeling and kriging method, with parameters optimized based on statistical validation metrics derived from the ENVI-met simulations. Finally, seasonal bioclimatic maps were produced to identify areas experiencing unfavorable thermal conditions. The spatial analysis revealed distinct seasonal patterns in the distribution of unfavorable thermal conditions across the Athens metropolitan area.

Keywords: ENVI-met; thermal index; micrometeorological measurements; kriging; Athens metropolitan area

Academic Editor: Eugene Rozanov

Received: 20 March 2026
Revised: 6 May 2026
Accepted: 14 May 2026
Published: 19 May 2026

1. Introduction

Urbanization requires effective hazard management to ensure safe and healthy living conditions [1]. Adverse thermal conditions, poor air, water and soil quality, excessive noise, waste-disposal issues, high-energy demands, and landscape degradation threaten

city residents' well-being. Among these, outdoor thermal stress conditions (heat) are of particular concern, as they are recognized by the World Health Organization [2] as one of the most dangerous natural hazards. Heat exposure is rising due to climate change and is intensified in cities by the heat island effect [2]. It is associated with a variety of health impacts, from mild heat-related symptoms to increased hospitalizations and mortality [3].

Thermal indices quantify the combined effects of air temperature, humidity, wind speed, and solar radiation on human physiology. They estimate the relationship between the thermal environment and well-being in terms of thermal sensation, comfort, or stress. For instance, applications of the modified Physiologically Equivalent Temperature (mPET) index have shown that prolonged heat stress exposure influences mortality risk in Athens [4]. Among the numerous indices available, Physiologically Equivalent Temperature (PET) and Universal Thermal Climate Index (UTCI) are two thermo-physiological indices that are well established in scientific literature and research [5,6].

Thermal indices are widely used in urban design [7] and environmental epidemiology [3]. Their application, however, typically relies on data from fixed meteorological stations, which may not accurately reflect urban microclimates, often leading to deviations in thermal stress classification. Furthermore, sparse station networks limit the ability to perform localized assessments. To overcome these limitations, modeling techniques have merged as powerful tools for analyzing urban thermal environments.

For accurate urban simulations, Huttner [8] outlined four key requirements: (1) high-resolution grids (<10 m) to capture the influence of buildings and vegetation; (2) detailed energy balance calculations for urban surfaces; (3) inclusion of both morphological and physiological characteristics of vegetation; and (4) prognostic equations to model atmospheric processes over time. The ENVI-met model [9] meets all these criteria, and it is widely used to assess the effects of urban planning on environmental variables [7,10,11]. ENVI-met is a three-dimensional microclimate model based on fluid dynamics and thermodynamics; it simulates air temperature, relative humidity, global radiation, and mean radiant temperature at high spatial resolution in urban environments [11]. The model is capable of reproducing surface–vegetation–atmosphere interactions without relying on in situ measurements—an important advancement in bioclimate assessment and urban planning [9]. Recent studies have further confirmed the model's capability to reproduce key thermal parameters and assess urban heat mitigation strategies under diverse climatic conditions, including Mediterranean environments [12,13].

Spatial variability in thermal conditions can be effectively visualized using maps that support public health [14], tourism [15], and urban design [16]. These maps are typically produced from spatial interpolation of meteorological data [17,18] or derived from gridded datasets such as ERA5-Land EURO-CORDEX [19,20]. Other studies rely on long-term climate observations or model outputs [21–23]. To ensure that these visualizations are both meaningful and practical, different levels of complexity in mapping techniques are employed, ranging from simple interpolation methods to advanced spatial estimations [15,22,24]. Moreover, the comparative performance of interpolation techniques, numerical modeling, and hybrid approaches has been explored, highlighting trade-offs between spatial accuracy, generalization capacity, and computational efficiency [25,26]. More recently, machine learning approaches have been introduced to improve the spatial prediction of urban thermal conditions. These include regression-based models, hybrid machine learning–kriging techniques, and deep learning approaches for urban temperature mapping [27–29]. While these approaches offer promising predictive performance, they often require large datasets and may lack the physical interpretability of process-based models.

However, existing studies generally treat microclimate modeling and spatial interpolation as separate processes, without explicitly utilizing high-resolution simulation

outputs as calibration input for spatial mapping. The present study develops a methodology for estimating the spatial variation in thermal conditions in the metropolitan area of Athens, Greece, by combining high-resolution simulations with surface meteorological data. Athens is a major city in the eastern Mediterranean—a region highly sensitive to climate change—identified as a thermal risk "hot spot" among 571 European cities [30]. Nationwide analyses confirm an increase in heat stress across Greece over the past three decades [19], consistent with the intensification of heat stress in Athens observed in long-term UTCI and PET records spanning nearly six decades [31], as well as in 124-year records of Thom's Discomfort Index, Humidex, and Heat Index [32].

This study proposes an ENVI-met-calibrated kriging framework that integrates microclimate simulations with meteorological observations in a unified modeling approach. By using ENVI-met outputs to inform and optimize a regression–kriging scheme, the method links microscale processes with city-scale thermal mapping while remaining computationally efficient. The main contributions of this work are: (a) the integration of high-resolution ENVI-met simulations as calibration input for spatial interpolation, (b) the optimization of kriging parameters to balance spatial accuracy and spatial coverage, and (c) the development of seasonally representative thermal stress maps, based on extensive field measurements and model validation.

The resulting framework provides a practical approach for assessing heat stress in urban areas and supporting mitigation and adaptation planning under both current and future climate conditions.

2. Materials and Methods

The overall framework of the methodology followed in this study is outlined below, and the corresponding workflow diagram is presented in Figure 1.

Meteorological data were collected using mobile weather stations during four field campaigns focused on thermal sensation [33–36]. The campaigns were conducted at eleven sites across the metropolitan area of Athens, Greece (Figure 2). In addition, data from the nearest fixed weather station to each campaign site were obtained for use in ENVI-met simulations.

ENVI-met was then used to estimate meteorological variables and thermal indices—specifically PET and UTCI—at the campaign locations. The accuracy of the high-resolution ENVI-met simulations was validated against in situ measurements collected during the field campaigns. PET and UTCI values were also calculated using weather station data and subsequently spatially interpolated using kriging.

Kriging interpolation was calibrated using ENVI-met outputs, and optimal parameters were selected based on statistical validation metrics. Finally, the spatial distribution of the thermal conditions across the wider area of Athens was estimated using the adjusted kriging method. This refined spatial interpolation approach was applied to map PET and UTCI values throughout Athens, enabling the identification of areas experiencing unfavorable thermal conditions.

A detailed description of each stage of the methodology is provided in the following subsections.

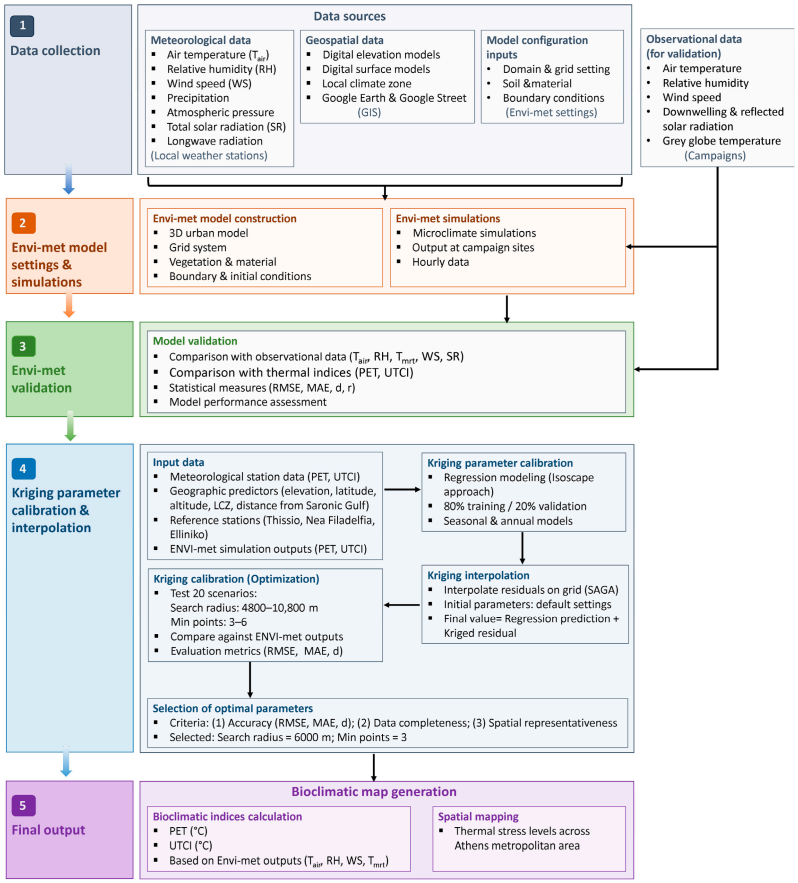

Figure 1. Research workflow diagram.

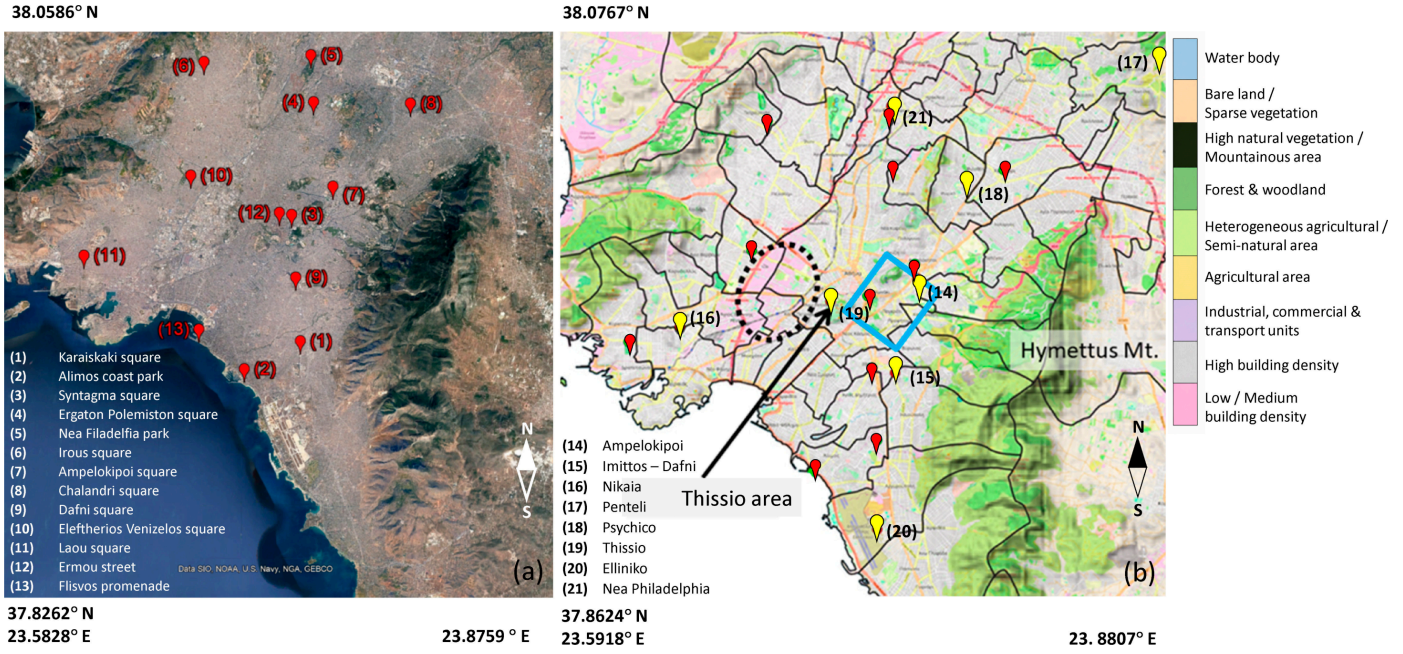

Figure 2. (**a**) Sites monitored in the field campaigns, and (**b**) map of the greater Athens area showing vegetation cover and meteorological stations operated by the National Observatory of Athens and the Hellenic National Meteorological Service (yellow dots). Red dots are the same in both panels. The map also highlights the Thissio green area, Hymettus Mountain (Mt.), a low-building-density area (black dotted circle), and Athens city center (blue square).

2.1. Data

2.1.1. Micrometeorological Data

Micrometeorological measurements were used to validate the ENVI-met simulations, ensuring reliable model performance under real-world conditions. Data were collected during four campaigns [33–36], all employing comparable methodologies. These campaigns covered thirteen urban public sites—including squares, parks and a promenade—across the Athens metropolitan area (Figure 2a). Mobile weather stations were installed at each site at a height of 1.1 m, representing pedestrian level. The recorded variables included air temperature (T_{air} [°C]), relative humidity (RH [%]), downwelling (SR_{down} [W/m^2]) and reflected (SR_{up} [W/m^2]) solar radiation, and gray globe temperature (T_{gl} [°C]), all measured at 1 min intervals. Each campaign consisted of continuous measurements over several hours during the day. In some cases, measurements were repeated at the same site to extend temporal coverage and better represent the full diurnal cycle. The campaigns spanned summer, winter and transitional seasons, with measurement durations varying accordingly: from 09:00 to 20:00 in summer, and from 09:00 to 18:00 in both winter and the transitional seasons. In total, 42 campaign days were analyzed in this study (Supplementary Materials Table S1).

For this study, data from eleven out of the thirteen campaigns were analyzed. Measurements from Ermou street were excluded due to its proximity to the Syntagma Square, and those from the Flisvos promenade (Figure 2a) were omitted because they lacked complete records for all three seasons.

2.1.2. Meteorological Station Data

Meteorological data from eight weather stations (Figure 2b) were used as initial conditions in ENVI-met simulations. The dataset included T_{air} (°C), RH (%), WS (m/s) and wind direction (WD [degrees]), precipitation (R [mm]) and atmospheric pressure (P [hPa]) for the corresponding campaign periods. Data at Penteli and Thissio stations were provided by the National Observatory of Athens (NOA), while those at Ampelokipoi, Imittos–Dafni, Nikaia and Psychico were provided by the weather stations network operated by the METEO unit at NOA (NOAAN) [37]. Data at Elliniko and Nea Philadelphia stations were provided by the Hellenic National Meteorological Service (HNMS). In addition, total solar radiation (SR [W/m^2]) and longwave radiation (LR [W/m^2]) were obtained from the actinometric stations of NOA (ASNOA), located at Penteli and Thissio. These are the only stations in the greater Athens area that routinely recorded shortwave and longwave radiation during the study period. Key information about all the stations is presented in the Supplementary Materials (Table S2).

2.1.3. Geospatial Data

Geospatial data were used to model the monitored sites in ENVI-met. Digital Elevation Models (DEMs) at 5 m resolution and Digital Surface Models (DSMs) at 0.8 m resolution were obtained from the Hellenic Cadastre, covering extended areas around each monitoring site. The heights of natural obstacles (e.g., trees and plants) and buildings were derived by subtracting DEM from DSM, resulting in relative height values above ground. All geospatial data processing and transformations were performed using the GIS (v3.10 LTR) software [38]. Additionally, the Local Climate Zone (LCZ) classification [39,40] was incorporated to characterize urban morphology. This dataset was obtained from the World Urban Database and Access Portal Tools (WUDAPT) project (https://doi.org/10.5281/zenodo.6364594, accessed on 18 May 2026).

The resulting models were verified and complemented with additional information on urban features—such as trees and buildings—using satellite imagery (Google Earth and Google Street [41]) and field observations.

2.2. ENVI-Met Model

2.2.1. Model Description

ENVI-met is a widely used and well documented bioclimatological modeling software that allows simulation of environmental conditions considering urban design impacts [9]. It is a three-dimensional microclimate model, based on fundamental laws of fluid dynamics and thermodynamics, designed to simulate complex surface-vegetation-atmosphere interactions in urban environments. The simulations require three main input components: (a) an "Area Input File" that holds the geometrical parameters of the modeled area, (b) a "Configuration File" that includes the initial calculation parameters and environmental conditions for the simulation, and (c) several "Database Files" that contain essential information such as vegetation type, soil stratification and water existence. The outputs environmental variables and thermal parameters such as Mean Radiant Temperature (T_{mrt} [°C]) at predefined spatial and temporal resolution. Thermal indices—including PET, UTCI, Predicted Mean Vote and Predicted Percentage of Dissatisfied (PMV/PPD), and Standard Effective Temperature (SET)—are calculated using the BioMET post-processing tool.

2.2.2. Model Set-Up

In this study, simulations were carried out using ENVI-met Science version 4.4.5 [42] and BioMET version 1.5 [43].

The campaign sites (Figure 2a) were digitally modeled by incorporating detailed information on buildings, vegetation, and soil types. Soil profiles and material properties are presented in Supplementary Materials Table S3, while domain characteristics are summarized in Table S4 [44].

Buildings were modeled using the Monde Editor. The default wall materials—which also applied to the roofs of apartment blocks—were applied, while terracotta roofs were assigned to residential buildings. The tallest building (Ampelokipoi Square) reached 53 m. The total model height was set at least twice the height of the tallest structure to ensure accurate airflow simulation.

Tree characteristics were defined using the Albero Editor, including tree height, crown diameter, leaf properties such as leaf area density (LAD) and foliage albedo, as well as Root Area Density (RAD). A significant number of trees were modeled across the domains, with Erg. Polemiston Square containing the highest number and totaling 420 3D plants. Each domain included four to nine different soil types. In urban squares of Ampelokipoi, Chalandri, and Keratsini, dominant soil profiles consisted mainly of asphalt or used/dirty concrete pavement. In contrast, the residential parks of Alimos and Nea Filadelfia, along with Erg. Polemiston Square, featured stony pavement and brick roads.

All domains used a horizontal resolution of 1.5 × 1.5 m. Vertically, a base resolution of 2 m was applied, but the lowest grid cell was divided into five subcells to more accurately represent measurement height (1.1 m).

Furthermore, to establish consistent lateral boundary conditions for the core model and keep numerical stability [45,46], four to twenty empty cells (depending on the domain) were added around the main model domain, filling the empty grid space with the same surface materials as the border already has. No nesting grid cells were applied. In certain domains, rotation of the model orientation was necessary to better represent the layout of buildings. For these cases, a clockwise rotation angle from North was specified and applied accordingly.

2.2.3. Model Simulations

The simulations were initiated at midnight to ensure stable atmospheric conditions [47,48]. To minimize the influence of model spin-up effects and initialization artifacts—such as unrealistic heat storage in urban surfaces—the initial 8–10 h of each simulation were excluded from the analysis. This spin-up period is commonly adopted in ENVI-met applications to allow the model to reach a dynamic equilibrium. Starting the simulations during the pre-dawn hours further supports the development of a consistent diurnal cycle, leading to a more reliable representation of daytime microclimatic conditions. This procedure was consistently applied across all the seasons, taking into account the urban nature of the study area and aligning with established practices in similar studies [49,50]. Although this approach increases the overall computational time, it significantly enhances the robustness and accuracy of the simulation outputs [51]. ENVI-met supports simple and full forced boundary conditions. The full forcing (advanced level) was used in this study, with meteorological station data applied at 30 min intervals to define initial conditions. Hourly raw data was converted to 30 min steps using linear interpolation. Constant time steps of 2 s and model output intervals of 60 min were selected. The measurement heights of meteorological stations recording T_{air}, RH, and WS direction were imported into the forcing manager editor to initialize the model's meteorological conditions. The roughness length z_0 at each station ranged from 0.1 to 1 m, reflecting typical urban and suburban values [52]. The Standard Turbulence Model (Standard TKE Model) was used for all the model simulations [53], while the multi-core CPU option was enabled to shorten the computational time.

In total, 42 campaign days were simulated, providing a dataset to validate the ENVI-met results. All three seasons—summer, winter and transient—were represented, with up to two days simulated per site and season. The simulation dates are provided in Supplementary Materials Table S1.

2.2.4. Model Validation

The ENVI-met simulations were validated both qualitatively and quantitatively using campaign data for T_{air}, RH, T_{mrt}, WS, and SR. The PET and UTCI simulations were also validated using the PET and UTCI calculated from campaign data. The qualitative validation was based on the time series comparisons between the ENVI-met simulations and in situ measurements. The quantitative validation employed standard statistical metrics: Root Mean Square Error (RMSE), Mean Absolute Error (MAE), index of agreement (d), and correlation coefficient (r), following the methodology of previous similar studies [45,54,55]. The MAE represents the amount of "error" in the modeled values (the absolute difference between the observed and simulated values); the RMSE measures overall accuracy, and it is calculated as the square root of the mean of the square of all of the "error"; the d represents the ratio of the mean square error and the potential error, ranging from 0 (no agreement) to 1 (perfect agreement); the r ranges from -1 to +1, indicating how strong the relationship is between the observed and the modeled values.

2.3. Thermal Indices

The RayMan Pro software (v3.1 Beta) [56,57] was used to calculate PET and UTCI from both mobile and fixed station data. The simulated PET and UTCI were derived using BioMET. Standard PET and UTCI classification scales (Supplementary Materials, Table S5) were applied in both the model and interpolation validation processes. The original scales were applied, rather than locally adapted versions for Athens [58], to allow direct comparison with other studies and ensure broader applicability of the findings.

2.4. Kriging Calibration and Interpolation

Kriging is a geostatistical interpolation technique that generates bioclimatic maps from sparsely distributed meteorological stations by considering both spatial distance and variation between data points. It is widely applied in soil science and geology [59]. To enhance the accuracy of the gridded meteorological fields, we applied the isoscape method [60,61]. First, an empirical regression model was constructed to capture the relationship between a biometeorological index at a certain location, key geographical and local factors—namely elevation, latitude, altitude, LCZ and distance from the Saronic Gulf—and the values of that index at three fixed locations (the meteorological stations at Thissio, Nea Filadelfia and Elliniko). The robustness of the proposed model structure was validated by comparing the coefficients calculated over repeated applications of the 80% development-20% validation sampling scheme. Furthermore, the development procedure was applied both seasonally and annually, with the seasonal approach yielding slightly better fit statistics. A final set of three seasonal models was developed using the full dataset.

The residuals—representing unexplained spatial variability—were interpolated across a regular grid using kriging. The empirically predicted component was also calculated over the same grid. The final dataset was derived by combining the interpolated residuals with the model estimates.

Kriging interpolation was performed in the System for Automated Geoscientific Analyses software (SAGA v2.1.4) [62], initially using default parameters (Supplementary Materials, Table S6). Further parameter details are available in SAGA help documentation [62].

To calibrate the kriging method and further optimize spatial accuracy, ENVI-met microclimatic outputs were used as reference data. Twenty kriging scenarios were tested by varying key parameters: the search radius (ranging from 4800 to 10,800 m) and the minimum number of points required for interpolation (ranging from 3 to 6). Each scenario was evaluated by comparing PET and UTCI values derived from interpolated meteorological inputs against high-resolution ENVI-met outputs. Evaluation metrics included RMSE, MAE, and d. The optimal configuration was then applied to estimate the spatial distribution of PET and UTCI across the Athens metropolitan area.

3. Results

3.1. Validation of ENVI-Met Model

Validation results showed good agreement between the ENVI-met-simulated T_{air} and in situ T_{air} measurements across all the model runs (Supplementary Materials Figure S1a). Underestimation mainly occurred during transitional and winter periods with maximum differences of 9.3 °C (15 March 2012, Erg. Polemiston Square) and 7.8 °C (12 January 2020, Chalandri Square). In contrast, summer simulations slightly overestimated T_{air}, with a maximum difference of 4.7 °C (20 July 2020, Syntagma Square).

The RH was systematically overestimated by ENVI-met, particularly in winter (Supplementary Materials Figure S1b), with a maximum deviation exceeding 40% (15 March 2012; Erg. Polemiston Square). Nevertheless, the model accurately reproduced the timing of extreme values. The simulated T_{mrt} corresponded well with observations (Supplementary Materials Figure S1c), except for summer, when maximum values were overestimated.

The WS showed significant discrepancies, with frequent overestimations of maximum values (Supplementary Materials Figure S1d). These differences may be attributed to neighboring obstacles and local wind-channeling effects amplified by ENVI-met, as well as measurement interferences from campaign participants. The SR was consistently overestimated (Supplementary Materials Figure S1e), possibly due to transient shading from clouds or pedestrians, or discrepancies between the simulated and actual obstacles

(e.g., trees and buildings). An additional contributing factor may be model limitations to calculate SR, such as the assumption of isotropic scattering of diffuse radiation and limited absorption of diffuse shortwave radiation by vegetation [63].

Thermal indices simulated by ENVI-met showed satisfactory agreement with monitored values for both PET and UTCI (Supplementary Materials Figure S1f,g). However, UTCI time series were incomplete due to the minimum WS requirement for its calculation (0.5 m/s at 10 m height) [56,57].

The quantitative validation of T_{air} yielded RMSE = 2.2 °C, MAE = 1.5 °C, and high agreement (d = r = 1.0) (Table 1), consistent with results from previous studies [64,65]. The RH validation produced RMSE = 17.3% and MAE = 14.4%, indicating notable divergence between ENVI-met simulations and in situ measurements. This discrepancy may be linked to the divergence also found in SR simulations, following a recent study that supported that the simulations of RH were significantly affected by solar radiation [55]. In situ RH values may also have been affected by wind-driven moisture transport. Nevertheless, a d value of 0.9 indicates that the model adequately captured RH dynamics.

Table 1. Validation of ENVI-met simulations for all 42 campaign days.

Variable	RMSE	MAE	d	r
T_{air} (°C)	2.2	1.5	1.0	1.0
RH (%)	17.3	14.4	0.9	0.7
T_{mrt} (°C)	14.4	11.1	0.8	0.6
WS (m/s)	0.8	0.6	0.5	0.3
SR (W/m^2)	471.4	372.3	0.4	0.1
PET (°C)	6.9	4.9	0.9	0.8
UTCI (°C)	4.7	3.5	0.9	0.9

Larger differences were found for T_{mrt}, WS, and SR. Validation of T_{mrt} produced RMSE = 14.4 °C and MAE = 11.1 °C. WS produced RMSE = 0.8 m/s, MAE = 0.6 m/s and d = 0.5. This poor agreement could be attributed to limitations of the ENVI-met model in representing real-time wind variability. The largest errors were found for SR (RMSE = 471.4 W/m^2, MAE = 372.3 W/m^2), consistent with earlier findings (~170 W/m^2 [55]), and yielded the lowest d and r values (Table 1).

For thermal indices, PET and UTCI (Table 1) showed acceptable consistency with in situ data. Although errors were relatively high (RMSE = 6.9 °C, MAE = 4.9 °C for PET; RMSE = 4.7 °C, MAE = 3.5 °C for UTCI), both indices showed strong agreement (d = 0.9 and r $\geq$ 0.8). Validation of categorical classifications showed better agreement for UTCI (RMSE = 0.7 °C, MAE = 0.5 °C) than PET (RMSE = 1.2 °C, MAE = 0.8 °C) with d = 0.9 for both. Contingency table analysis showed that PET correctly predicted all the categories of its assessment scale except −4 (Figure 3a), while UTCI successfully reproduced categories 0, +1, and +2 (Figure 3b).

Overall, ENVI-met simulations using the full-forcing option reproduced micrometeorological and thermal conditions in open urban spaces of Athens with satisfactory accuracy. Among the evaluated variables, T_{air} showed the highest reliability, which is particularly important given its strong influence on human thermal perception [48].

3.2. Kriging Calibration

Kriging parameters were adjusted to reproduce ENVI-met simulations of PET and UTCI at the monitored sites after incorporating the regression estimates. Twenty interpolation runs were performed by varying the search radius (4800–10,800 m) and the minimum points parameters (3–6). The interpolated PET and UTCI values were evaluated against

high-resolution ENVI-met outputs using RMSE, MAE, and d. The statistical results for all the configurations are presented in Table 2.

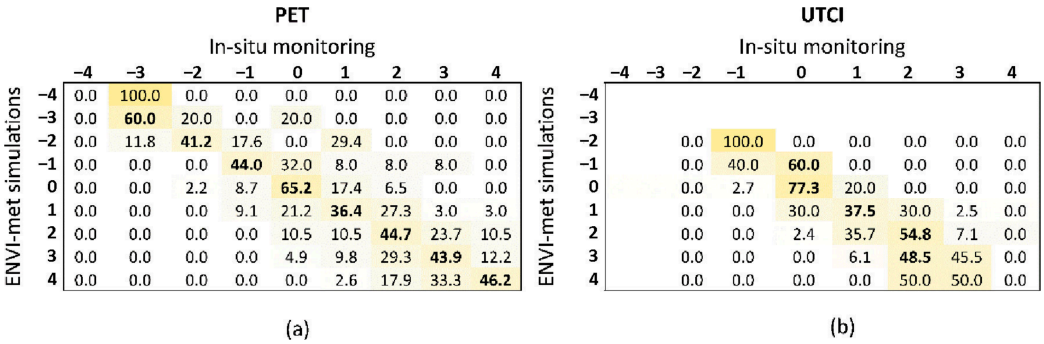

Figure 3. Distribution of (**a**) PET and (**b**) UTCI categories of their assessment scales according to ENVI-met simulations against in situ measurements. Rows add to 100%, bold values indicate the number in diagonal, gradient shading darkens per 10%. The gamma statistic was 0.78 for PET and 0.899 for UTCI, $p < 0.001$.

Table 2. Validation metrics and data completeness for interpolated PET and UTCI using various kriging radii (in m) and minimum number of neighboring points (min points).

	PET				UTCI			
Root Mean Squared Error (RMSE)								
Search Radius (m)/ Min Points	**3**	**4**	**5**	**6**	**3**	**4**	**5**	**6**
4800	6.7	6.3	6.5	5.9	6.6	6.2	6.4	4.3
6000	6.5	6.7	7.0	7.6	6.1	6.3	6.5	7.1
7200	6.5	6.6	6.6	6.8	6.1	6.1	6.2	6.4
8400	6.5	6.6	6.6	6.7	6.1	6.1	6.1	6.1
10,800	6.4	6.4	6.4	6.4	6.0	6.0	6.0	6.0
Mean Absolute Error (MAE)								
4800	5.4	5.2	5.3	4.4	5.3	4.8	5.0	3.4
6000	5.3	5.4	5.7	6.3	4.9	5.0	5.0	5.5
7200	5.3	5.4	5.4	5.6	4.8	4.9	5.0	5.0
8400	5.3	5.4	5.4	5.4	4.8	4.9	4.8	4.9
10,800	5.2	5.2	5.2	5.2	4.7	4.7	4.7	4.7
Index of Agreement (d)								
4800	0.9	0.9	0.9	0.8	0.9	0.9	0.9	0.8
6000	0.9	0.9	0.9	0.8	0.9	0.9	0.9	0.9
7200	0.9	0.9	0.9	0.9	0.9	0.9	0.9	0.9
8400	0.9	0.9	0.9	0.9	0.9	0.9	0.9	0.9
10,800	0.9	0.9	0.9	0.9	0.9	0.9	0.9	0.9
Completeness (%)								
4800	46	29	11	5	37	17	13	3
6000	67	54	33	24	51	41	32	19
7200	73	67	59	47	52	50	47	36
8400	73	70	67	59	52	51	51	51
10,800	78	78	75	75	54	54	54	54

RMSE, MAE, and d values remained relatively consistent across parameter combinations with mean RMSE ≈ 6.5, MAE ≈ 5.5, and d = 0.9. The configuration with a 4800 m radius and six points achieved the lowest RMSE (5.9) and MAE (4.4), but with slightly

reduced agreement (d = 0.8). Conversely, the 6000 m radius with six points produced the highest RMSE (7.6) and MAE (6.3), also with d = 0.8.

Data completeness of the kriging outputs was also assessed. As expected, a minimum of three neighboring points provided the highest completeness, while six points yielded the lowest (Table 2). Applying a 50% threshold as the criterion for acceptable spatial coverage, the kriging configuration with a 6000 m search radius and a minimum of three neighboring points was identified as optimal. Although larger search radii (e.g., 10,800 m) yielded slightly improved statistical metrics, their use introduces greater spatial heterogeneity and may lead to oversmoothing of local variability.

The selected configuration (6000 m, 3 points) provides the best balance between statistical performance, spatial coverage, and preservation of local-scale variability. This configuration achieved a coverage ratio of 11.2 PET (8.5 UTCI) per kilometer of search radius, calculated as completeness divided by radius in kilometers (i.e., 67/6 for PET and 51/6 for UTCI). By comparison, the (7200 m, 3 points) configuration yields 10.1 PET (7.2 UTCI), offering no meaningful gain in accuracy (~2% higher RMSE/MAE) relative to the 10,800 m case, which had lower coverage (7.2 PET, 5 UTCI per km). Thus, the selected setup ensures reliable spatial representation while maintaining sensitivity to local variability, particularly in areas with a sparse network of meteorological stations.

3.3. Validation of the Interpolation Method

An obvious question would be "Why not use ENVI-met to obtain the gridded bioclimatic indices across the entire area instead of resorting to interpolation?". The answer would be that the computational resources—particularly processing time—required for such simulations would limit their applicability for practical implementation. A possible alternative would be to apply ENVI-met at a coarse resolution. In this context, a domain of about 1 × 1 km was selected to represent a large area of the center of Athens, including the most frequently visited squares of the city. The selection criteria included population density, landscape diversity, and the area's importance as a tourist destination, especially in summer months when extreme thermal conditions are encountered. The results obtained for this domain could therefore be considered representative of the entire urban area of Athens. The simulation domain consisted of 214 × 214 grid cells horizontally and 50 vertical levels, with a spatial resolution of 5 × 5 × 5 m, resulting in a total horizontal extent of 1070 × 1070 m, covering an area of about 1,144,900 m^2. The lowest gridbox was split into 5 subcells consistent with the fine-resolution simulations described above. The soil profiles, construction materials, and vegetation characteristics, along with the corresponding satellite imagery, are presented in Supplementary Materials Figure S2.

Three full forcing simulations—one for each season (summer, winter, and a transient period)—were carried out. All the other model settings were kept consistent with those used in the fine model simulations.

The interpolation method described above was quantitatively validated using the statistical metrics RMSE and MAE for the PET index. About 100 interpolated PET values, covering the coarse simulation domain, were compared against corresponding ENVI-met outputs. Due to the difference in spatial resolution (90 × 90 m for interpolation versus 5 × 5 m for ENVI-met), each interpolated value was compared with the mean PET value of 324 ENVI-met grid points (18 × 18 cells). Each interpolated grid point was positioned at the center of the 18 × 18 modeled grid point block. Building grid points were excluded from the calculations. Since the category of index assessment scales is of particular importance for this project, the validation procedure was also performed for thermal sensation/stress classifications.

The results suggest that the selected kriging parameterization produces a spatial distribution of PET that aligns well with the coarser simulated outputs, both in terms of index values and their corresponding categories on the assessment scales. In most cases, the thermal stress category predicted by kriging matches the one simulated by ENVI-met, or at worst, falls into the adjacent category. According to the contingency table analysis, the highest percentages of exact agreement between ENVI-met and the interpolation was 38.2% in winter, 4.5% in the transient season, and 78.7% in summer. When including adjacent categories, agreement reached 100%. Notably, the best performance was observed during the summer period, indicating that the calibrated kriging approach is particularly effective under conditions of elevated thermal stress, when accurate spatial representation is most critical.

3.4. Bioclimatic Maps

Bioclimatic maps were developed to identify urban areas of Athens experiencing unfavorable heat-related conditions. Spatial interpolation of PET and UTCI was performed using a combined regression-kriging method, parameterized from ENVI-met simulations (search radius = 6000 m, minimum search point = 3), as described in Section 3.2. The analysis focused on the hour of maximum PET/UTCI values for each season. To determine these peak hours, meteorological data from surface weather stations (42 campaign days) were processed with the RayMan model to compute hourly PET and UTCI. The maximum mean hourly PET/UTCI values occurred at 14:00 LST in summer, 13:00 LST in transient, and 12:00 LST in winter.

Kriged values of T_{air}, RH, SR and WS at these hours (14:00 LST in summer, 13:00 LST in transient and 12:00 LST in winter) were then used to calculate PET and UTCI at each grid point across the study domain. The resulting PET and UTCI maps for the summer season are presented in Figure 4a,d.

PET exceeded 35 °C across much of the metropolitan area, corresponding to "hot" and "very hot" categories according to the PET classification scale [66], with maximum PET reaching 43 °C and UTCI peaking at about 38 °C, corresponding to "very strong heat stress". Areas experiencing unfavorable thermal conditions were primarily located in the eastern Athens basin, particularly along the western side of the mountain Hymettus. During summer, prevailing northeasterly winds (Etesians) dominate Athens [67–69]. This pattern is also confirmed by observations at Thissio station, where about 72% of the 42 campaign days were characterized by northerly to northeasterly winds. These downslope winds lead to warmer and more unfavorable thermal conditions on the leeward side of Hymettus, similar to patterns observed in other regions of Greece with complex topography [70]. Conversely, lower PET and UTCI values were calculated over the central and southwestern parts of Athens (PET $\approx$ 40 °C and UTCI $\approx$ 35 °C). The lowest values were found in the southwestern areas, likely due to the influence of sea breeze circulation, particularly the prevailing southwestern winds that help moderate summer heat along the western Attica coast.

The spatial distributions of PET and UTCI during the transient season (Figure 4b,e) at 13:00 LST show relatively unfavorable thermal conditions in the southwestern regions with maximum PET reaching 37 °C (classified as "hot") and UTCI 33 °C (classified as "very strong heat stress"). Lower values of PET and UTCI were observed in the rest of the metropolitan area of Athens. The lowest PET and UTCI values occurred during winter at 12:00 LST (Figure 4c,f). In winter, PET indicated "neutral" thermal conditions (18 °C < PET < 23 °C) across most of Athens, with "slightly warm" conditions (23 °C < PET < 29 °C) occurring in the northeastern suburbs. UTCI showed a similar spatial pattern, with most areas falling into the "no thermal stress" category (9 °C < UTCI < 26 °C).

Notably, across all the seasons, slightly lower PET and UTCI values were observed in the green areas within the city center and in the western districts (Figure 4a,d). In the green area of Thissio, near Filopappou Hill, PET values were about 2–5 °C lower than those in the surrounding areas. This cooling effect can be attributed to the shading provided by dense tree cover and vegetation. A similar pattern was observed in the western districts, where building density is notably low. In contrast, areas of high building density—such as the city center and the northeastern and southwestern districts—consistently exhibited elevated PET and UTCI values across all the seasons.

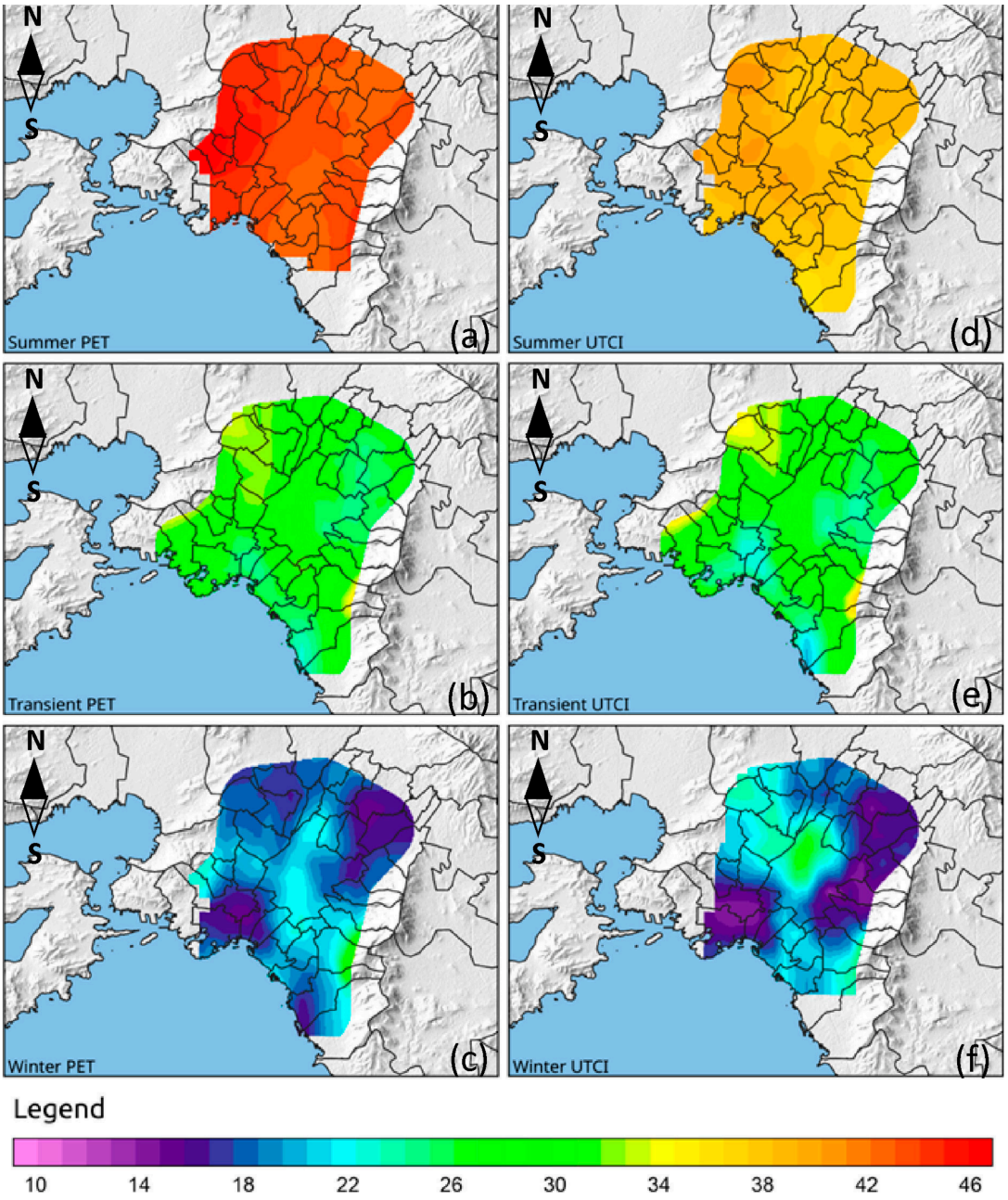

Figure 4. Spatial distribution of PET (°C) and UTCI (°C) across the Athens metropolitan area for different seasons: PET in (**a**) summer, (**b**) the transitional season, and (**c**) winter; and UTCI in (**d**) summer, (**e**) the transitional season, and (**f**) winter. Values represent seasonally averaged conditions based on the 42 campaign days, calculated at the hour of maximum thermal stress for each season (14:00 LST in summer, 13:00 LST in the transitional season, and 12:00 LST in winter).

4. Discussion

This study presents a methodology for mapping thermal conditions across the Athens metropolitan area. It integrates micrometeorological observations, meteorological station data, and high-resolution ENVI-met simulations. Beyond its application to Athens, the approach advances existing methods by using ENVI-met outputs to calibrate and optimize a regression–kriging interpolation scheme, effectively linking microscale processes with city-scale thermal mapping. This integration enhances the reliability of spatial thermal assessments while maintaining computational efficiency compared to large-scale microclimate simulations. Although applied to a Mediterranean urban environment, the methodology relies on widely available data and standard modeling tools, making it transferable to other cities, particularly those with limited observational networks.

The ENVI-met model successfully simulated thermal indices at open urban sites in Athens, demonstrating its effectiveness as a reliable tool for analyzing thermal conditions in urban environments. These findings are consistent with previous studies [12,71–73]. In line with Elraouf et al. [71], the model showed its highest validation performance for air temperature, which is widely recognized as the most influential factor in shaping thermal perception [74]. In contrast, lower validation scores were found for wind speed and total solar radiation, mainly due to shading effects from surrounding structures and/or pedestrian interference. Similar limitations have been reported in prior research, where ENVI-met tends to overestimate wind speed and faces challenges in modeling longwave radiation fluxes [75] and mean radiant temperature [76].

Previous studies have demonstrated that ENVI-met outputs are highly sensitive to vegetation structure (e.g., LAD), surface reflectivity (albedo), and soil parameters, which significantly affect mean radiant temperature and subsequently PET and UTCI values [77,78]. Moreover, sensitivity analyses have shown that these parameters exhibit non-linear interactions, reinforcing the need to interpret simulation outputs as scenario-dependent rather than deterministic predictions [79].

Despite the notable discrepancies between the simulated and observed wind speed values, their influence on the derived thermal indices (PET and UTCI) was limited. Both indices show strong agreement between the ENVI-met simulations and in situ measurements, indicating that thermal conditions were accurately reproduced. This is supported by the validation metrics, where PET and UTCI exhibit high agreement with observations, despite larger errors in individual variables such as solar radiation, wind speed, and mean radiant temperature. Further evidence is provided in Supplementary Figure S1, where substantial deviations in wind speed are not reflected in corresponding deviations in PET and UTCI, particularly when air temperature is accurately reproduced. This behavior can be attributed to the stronger dependence of these indices on air temperature compared to WS [80]. Similar findings were reported by Elraouf et al. [71], who showed that although ENVI-met has limited accuracy in simulating wind speed, it reliably captured PET, with strong agreement against field-based observations. Moreover, the kriging interpolation was calibrated using ENVI-met–derived PET and UTCI values—which exhibited low deviations from observations—rather than individual meteorological variables. This approach implicitly incorporates and compensates for model-related discrepancies, including those associated with wind speed, thereby minimizing their propagation into the final bioclimatic maps.

The fine-tuning/calibration of the kriging parameters using ENVI-met simulations yielded satisfactory results, indicating that the proposed interpolation method, using calibrated kriging, is effective in spatial interpolation of thermal conditions. Seasonal bioclimatic maps were developed and validated against ENVI-met simulations conducted over a coarser domain. The interpolated maps closely matched the coarse ENVI-met simulations with the predicted thermal conditions classified within the same or adjacent

thermal sensation categories on the index assessment scale. Validation scores were higher during summer and lower in the transient season, indicating that the kriging calibration was particularly effective during periods of elevated thermal stress. This difference may be related to the more stable and persistent meteorological conditions typically observed in summer (i.e., prevailing northeasterly winds, anticyclonic circulation, low cloud cover, and relatively consistent solar radiation), which likely produce more consistent spatial patterns that are easier to capture by the ENVI-met simulations. In contrast, the transient season is often associated with increased atmospheric variability, including changes in wind patterns and radiation conditions, which can introduce greater spatial heterogeneity and uncertainty.

The resulting bioclimatic maps depicted the spatial distribution of thermal conditions across the Athens metropolitan area, highlighting the seasonal variability of areas experiencing unfavorable thermal conditions. In summer, increased thermal load was primarily found in the eastern regions, particularly along the western side of the mountain Hymettus. During the transient season, increased thermal load was found in the southwestern regions, while in winter, relatively warmer thermal conditions were found in the northeast suburbs. This seasonal variation could be attributed, at least in part, to the region's topography. Notably, in all the seasons, slightly lower PET and UTCI values were observed in green areas of the city center and in the western districts, where building density is relatively low. Conversely, areas with high building density—particularly in the city center and the northeastern and southwestern center districts—exhibit consistently seasonal higher values of PET and UTCI. These findings align with prior research emphasizing the importance of vegetation coverage and urban form in reducing thermal stress and improving outdoor thermal comfort in built environments [16].

As with most studies, the current study is subject to certain limitations that introduce uncertainty into the results. First, the relatively sparse network of meteorological stations may not fully capture the spatial variability of thermal conditions across the study area, potentially affecting the accuracy of the interpolated variables. Second, in situ measurements prioritized high-building density areas with significant pedestrian traffic and thermal exposure, such as dense urban spaces, squares, and parks; consequently, low-density areas were underrepresented in the network due to site selection priorities. Moreover, the limited duration for certain measurement campaigns may constrain the overall robustness of the statistical validation. In addition, model-related uncertainties arise from known limitations of ENVI-met, particularly in simulating wind speed, solar radiation, and mean radiant temperature and its sensitivity to key input parameters such as leaf area density and surface albedo, which may carry over into the estimation of thermal indices. The use of standard PET and UTCI assessment scales rather than the locally calibrated thresholds for Athens ensures comparability with international studies; however, it may not fully account for the physiological acclimatization and behavioral adaptation of local populations to Mediterranean climatic conditions [81]. Consequently, the application of standardized scales may lead to an over- or underestimation of actual thermal stress.

The sensitivity analysis of the kriging parameters (e.g., search radius and number of neighboring points) demonstrated that interpolation performance remains relatively stable across a range of configurations, indicating robustness of the overall approach. Nevertheless, a full uncertainty propagation and sensitivity analysis—including the combined effects of model assumptions, input data quality, and interpolation parameters—was beyond the scope of this study. Finally, the interpolation and bioclimatic map development relied on a somewhat coarse data grid, as our focus was on developing an easy-to-apply framework. It should be noted that the spatial resolution of the bioclimatic maps reflects this methodological focus, aiming at the development of a transferable interpolation approach

rather than the identification of fine-scale urban hot spots. Therefore, the results are more appropriate for city-scale assessments. In this context, a portion of the environmentally caused variability was indirectly taken into account through the kriging of the regression modeling residuals. Further limitations include the exclusion of anthropogenic heat emissions from the simulations, the absence of future climate projections, and the method's reduced applicability in high-density, canyon-style urban blocks.

Despite these limitations, the presented methodology is promising, as it combines field measurements with high-resolution model simulations. All data were sourced from the National Observatory of Athens and the Hellenic National Meteorological Service, ensuring their accuracy. The original assessment scales of PET and UTCI were used to facilitate comparisons and to ensure the broad applicability of this study's findings. The simplicity of the approach, combined with the successful validation of the results, indicates that this method can effectively identify areas experiencing unfavorable thermal conditions. Future work could incorporate locally calibrated PET and UTCI assessment thresholds for Athens. Such an approach would better reflect local thermal perception and enhance the applicability of bioclimatic maps.

Implications for Urban Planning and Public Health

The methodology developed in this study represents a useful tool for visualizing thermal conditions across the Athens metropolitan area and can support applications in urban planning, public health, and climate adaptation strategies. Similar approaches have already been applied in practice to inform the design and placement of mitigation measures such as urban greenery, shading structures, and material modifications [82] and to evaluate the effectiveness of climate adaptation strategies, including green infrastructure interventions [83]. In the field of public health, thermal indices have also been applied to assess population exposure to heat stress [3].

In the context of this study, the identification of zones with varying levels of thermal stress enables the development of targeted, location-specific mitigation strategies. Based on the generated bioclimatic maps, the eastern Athens basin—where persistent high thermal stress is observed—would benefit from interventions prioritizing the enhancement of ventilation corridors and the integration of vertical greenery systems to reduce heat accumulation and improve airflow. In the southwestern coastal areas, where sea-breeze effects moderate thermal conditions, urban design should focus on optimizing waterfront spaces by preserving open wind pathways and incorporating shaded recreational zones to maximize thermal comfort. In densely built historic areas of the city center, the implementation of permeable pavements, increased tree canopy cover, and shading infrastructures (e.g., pergolas and reflective materials) is recommended to mitigate heat stress at the pedestrian level.

Beyond urban design, the bioclimatic maps have direct applications in public health and urban management. They can support real-time heat risk assessment by identifying high-exposure zones during extreme heat events, contributing to early warning systems and targeted intervention planning for vulnerable populations. Furthermore, these maps can inform tourism planning by identifying thermally comfortable areas and optimal visiting periods, enhancing visitor experience while reducing heat-related risks.

It should be noted that the primary aim of this study was to develop and demonstrate the proposed methodology. For operational decision-making, bioclimatic maps should ideally be generated using long-term climatic datasets to ensure robustness and representativeness of prevailing thermal conditions.

5. Conclusions

This study presents a tested and applied methodology for mapping urban thermal conditions by combining high-resolution ENVI-met simulations, in situ micrometeorological measurements, and interpolated biometeorological indices calculated from weather station data. The approach successfully captures the spatial patterns of human thermal conditions across the Athens metropolitan area, particularly during summer when thermal stress is most intense. The ENVI-met model proved effective in simulating thermal indices, while the combined modeling-calibrated kriging approach allowed for accurate and spatially continuous mapping. The results underscore the critical role of vegetation cover, urban morphology, and topography in shaping urban thermal conditions. Overall, the proposed methodology provides a practical tool for urban planning, public health, and climate adaptation by identifying areas of elevated thermal stress and supporting the development of targeted mitigation strategies.

Supplementary Materials: The following supporting information can be downloaded at https://www.mdpi.com/article/10.3390/atmos17050522/s1. Figure S1: Qualitative validation results (simulated versus monitored on-site) for all simulations throughout the study seasons (summer, winter, transient) for (a) air temperature (T_{air}), (b) relative humidity (RH), (c) mean radiant temperature (T_{mrt}), (d) wind speed (WS), (e) total solar radiation (SR), (f) Physiologically Equivalent Temperature (PET) and (g) Universal Thermal Climate Index (UTCI); Figure S2: Areas input files 2D and 3D view of land materials and structured environment plan of the simulated coarse domains with the satellite imagery (Google Earth); Table S1: Number of days used for model simulation, for each season and monitoring site in the field campaigns; Table S2: Meteorological stations operated by meteorological services and institutions whose data are used in the project; Table S3: Two-dimensional views of the Area Input Files showing land surface materials and the built environment layout within the simulated domains, overlaid on satellite imagery (Google Earth); Table S4: Model geometry, tallest building height, and the number of distinct soil profiles and 3D vegetation elements of each study area; Table S5: Assessment scales of PET and UTCI; Table S6: Kriging settings as applied to SAGA software for the standard process.

Author Contributions: Conceptualization, I.K., K.P. and S.L.; methodology, I.K., K.P. and S.L.; software, I.K. and A.B.; validation, I.K.; formal analysis, I.K. and S.L.; investigation, I.K., K.P., S.L. and A.T.; resources, I.X.T., K.L., B.E.P., D.F. and V.K.; data curation, all authors; writing—original draft preparation, I.K. and K.P.; writing—review and editing, S.L., A.T., A.B., I.X.T., K.L., B.E.P., D.F. and V.K.; visualization, I.K., K.P. and A.B.; supervision, K.P. and S.L.; project administration, I.K., K.P. and S.L.; funding acquisition, K.P., K.L. and V.K. All authors have read and agreed to the published version of the manuscript.

Funding: This research was funded by the Hellenic Foundation for Research and Innovation (HFRI), the General Secretariat for Research and Technology (GSRT), under grant agreement No 146, and the project "Support for upgrading the operation of the National Network for Climate Change—Climpact" (Grant Agreement: 2023NA11900001, ΟΠΣ_5201588).

Institutional Review Board Statement: Not applicable.

Informed Consent Statement: Not applicable.

Data Availability Statement: The datasets used during the current study can be made available upon reasonable request.

Acknowledgments: The authors would like to acknowledge the Hellenic National Meteorological Service for providing meteorological data.

Conflicts of Interest: The authors declare no conflicts of interest. The funders had no role in the design of the study; in the collection, analyses, or interpretation of data; in the writing of the manuscript; or in the decision to publish the results.

References

1. Streimikiene, D. Environmental Indicators for the Assessment of Quality of Life. *Intellect. Econ.* **2015**, *9*, 67–79. [CrossRef]
2. WHO (World Health Organization). Health Topics, Heatwaves. Available online: https://www.who.int/health-topics/heatwaves#tab=tab_1 (accessed on 15 March 2026).
3. Pantavou, K.; Fillon, A.; Li, L.; Maniadis, Z.; Nikolopoulos, G.K. Thermal Indices for Assessing the Impact of Outdoor Thermal Environments on Human Health: A Systematic Review of Epidemiological Studies. *Int. J. Biometeorol.* **2025**, *69*, 1843–1866. [CrossRef]
4. Giannaros, C.; Economou, T.; Parliari, D.; Galanaki, E.; Kotroni, V.; Lagouvardos, K.; Matzarakis, A. A Thermo-Physiologically Consistent Approach for Studying the Heat-Health Nexus with Hierarchical Generalized Additive Modelling: Application in Athens Urban Area (Greece). *Urban Clim.* **2024**, *58*, 102206. [CrossRef]
5. de Freitas, C.R.; Grigorieva, E.A. A Comprehensive Catalogue and Classification of Human Thermal Climate Indices. *Int. J. Biometeorol.* **2015**, *59*, 109–120. [CrossRef] [PubMed]
6. Potchter, O.; Cohen, P.; Lin, T.P.; Matzarakis, A. Outdoor Human Thermal Perception in Various Climates: A Comprehensive Review of Approaches, Methods and Quantification. *Sci. Total Environ.* **2018**, *631–632*, 390–406. [CrossRef]
7. Tseliou, A.; Tsiros, I.X. Modeling Urban Microclimate to Ameliorate Thermal Sensation Conditions in Outdoor Areas in Athens (Greece). *Build. Simul.* **2016**, *9*, 251–267. [CrossRef]
8. Huttner, S. Further Development and Application of the 3D Microclimate Simulation ENVI-Met. Ph.D. Thesis, Johannes Gutenberg University of Mainz, Mainz, Germany, 2012.
9. Bruse, M.; Fleer, H. Simulating Surface-Plant-Air Interactions inside Urban Environments with a Three Dimensional Numerical Model. *Environ. Model. Softw.* **1998**, *13*, 373–384. [CrossRef]
10. Johansson, E.; Thorsson, S.; Emmanuel, R.; Krüger, E. Instruments and Methods in Outdoor Thermal Comfort Studies—The Need for Standardization. *Urban Clim.* **2014**, *10*, 346–366. [CrossRef]
11. Salata, F.; Golasi, I.; de Lieto Vollaro, R.; de Lieto Vollaro, A. Urban Microclimate and Outdoor Thermal Comfort. A Proper Procedure to Fit ENVI-Met Simulation Outputs to Experimental Data. *Sustain. Cities Soc.* **2016**, *26*, 318–343. [CrossRef]
12. Fiorillo, E.; Brilli, L.; Carotenuto, F.; Cremonini, L.; Gioli, B.; Giordano, T.; Nardino, M. Diurnal Outdoor Thermal Comfort Mapping through Envi-Met Simulations, Remotely Sensed and In Situ Measurements. *Atmosphere* **2023**, *14*, 641. [CrossRef]
13. Aleksandrowicz, O.; Saroglou, T.; Pearlmutter, D. Evaluation of Summer Mean Radiant Temperature Simulation in ENVI-Met in a Hot Mediterranean Climate. *Build. Environ.* **2023**, *245*, 110881. [CrossRef]
14. Hu, K.; Yang, X.; Zhong, J.; Fei, F.; Qi, J. Spatially Explicit Mapping of Heat Health Risk Utilizing Environmental and Socioeconomic Data. *Environ. Sci. Technol.* **2017**, *51*, 1498–1507. [CrossRef] [PubMed]
15. Matzarakis, A.; Rudel, E.; Zygmuntowski, M.; Koch, E. Bioclimatic Maps for Tourism Purposes. *Phys. Chem. Earth Parts A/B/C* **2010**, *35*, 57–62. [CrossRef]
16. Colaninno, N.; Salvati, A.; Lopez-Besora, J.; Morganti, M. District-Scale Cumulative Heat Stress Mapping Using Very-High-Resolution Spatiotemporal Simulation. *Sustain. Cities Soc.* **2025**, *130*, 106498. [CrossRef]
17. Environmental Systems Research Institute (ESRI). *ArcGIS 9. What Is ArcGIS 9.1?* Environmental Systems Research Institute: Redlands, CA, USA, 2005. Available online: http://www.esri.com/ (accessed on 16 March 2026).
18. Neteler, M.; Mitasova, H. *Open Source GIS: A GRASS GIS Approach*; Springer: Cham, Switzerland, 2008; pp. 1–406. [CrossRef]
19. Pantavou, K.; Kotroni, V.; Kyros, G.; Lagouvardos, K. Thermal Bioclimate in Greece Based on the Universal Thermal Climate Index (UTCI) and Insights into 2021 and 2023 Heatwaves. *Theor. Appl. Climatol.* **2024**, *155*, 6661–6675. [CrossRef]
20. Pantavou, K.; Kotroni, V.; Lagouvardos, K.; Kyriakou, P. Future Changes of Bioclimate in Greece: Variations in Thermal Stress According to the Universal Thermal Climate Index (UTCI). *Sci. Total Environ.* **2025**, *980*, 179514. [CrossRef]
21. Ryan, S.J. Mapping Thermal Physiology of Vector-Borne Diseases in a Changing Climate: Shifts in Geographic and Demographic Risk of Suitability. *Curr. Environ. Health Rep.* **2020**, *7*, 415–423. [CrossRef]
22. Lin, T.P.; Chen, Y.C.; Matzarakis, A. Urban Thermal Stress Climatic Mapping: Combination of Long-Term Climate Data and Thermal Stress Risk Evaluation. *Sustain. Cities Soc.* **2017**, *34*, 12–21. [CrossRef]
23. Boehm, J.; Niell, A.; Tregoning, P.; Schuh, H. Global Mapping Function (GMF): A New Empirical Mapping Function Based on Numerical Weather Model Data. *Geophys. Res. Lett.* **2006**, *33*, L07304. [CrossRef]
24. Ketterer, C.; Matzarakis, A. Mapping the Physiologically Equivalent Temperature in Urban Areas Using Artificial Neural Network. *Landsc. Urban Plan.* **2016**, *150*, 1–9. [CrossRef]
25. Hassani, A.; Santos, G.S.; Schneider, P.; Castell, N. Interpolation, Satellite-Based Machine Learning, or Meteorological Simulation? A Comparison Analysis for Spatio-Temporal Mapping of Mesoscale Urban Air Temperature. *Environ. Model. Assess.* **2024**, *29*, 291–306. [CrossRef]
26. Brabant, C.; Dubreuil, V.; Dufour, S. Evaluation of Spatial Interpolation Techniques for Urban Heat Island Monitoring in Small and Medium Sized Cities. *Front. Built Environ.* **2024**, *10*, 1455047. [CrossRef]

27. Delgado-Enales, I.; Lizundia-Loyola, J.; Molina-Costa, P.; Del Ser, J. A Machine Learning Approach for the Efficient Estimation of Ground-Level Air Temperature in Urban Areas. *Urban Clim.* **2025**, *61*, 102415. [CrossRef]
28. Briegel, F.; Wehrle, J.; Schindler, D.; Christen, A. High-Resolution Multi-Scaling of Outdoor Human Thermal Comfort and Its Intra-Urban Variability Based on Machine Learning. *Geosci. Model Dev.* **2024**, *17*, 1667–1688. [CrossRef]
29. AlShafeey, M. Unraveling Climate Trends in the Mediterranean: A Hybrid Machine Learning and Statistical Approach. *Model. Earth Syst. Environ.* **2024**, *10*, 6255–6277. [CrossRef]
30. Guerreiro, S.B.; Dawson, R.J.; Kilsby, C.; Lewis, E.; Ford, A. Future Heat-Waves, Droughts and Floods in 571 European Cities. *Environ. Res. Lett.* **2018**, *13*, 034009. [CrossRef]
31. Katavoutas, G.; Founda, D. Intensification of Thermal Risk in Mediterranean Climates: Evidence from the Comparison of Rational and Simple Indices. *Int. J. Biometeorol.* **2019**, *63*, 1251–1264. [CrossRef]
32. Psiloglou, B.E.; Gkinis, N.; Giannakopoulos, C. High-Resolution Temporal Variation of Thermal Discomfort Indices in the Eastern Mediterranean City of Athens, Greece, Since the Beginning of the 20th Century (1901–2024). *Climate* **2025**, *13*, 210–255. [CrossRef]
33. Pantavou, K.; Theoharatos, G.; Santamouris, M.; Asimakopoulos, D. Outdoor Thermal Sensation of Pedestrians in a Mediterranean Climate and a Comparison with UTCI. *Build. Environ.* **2013**, *66*, 82–95. [CrossRef]
34. Tseliou, A.; Tsiros, I.X.; Nikolopoulou, M.; Papadopoulos, G. Outdoor Thermal Sensation in a Mediterranean Climate (Athens): The Effect of Selected Microclimatic Parameters. *Archit. Sci. Rev.* **2016**, *59*, 190–202. [CrossRef]
35. Nikolopoulou, M. *Designing Open Space in the Urban Environment: A Bioclimatic Approach*; Centre for Renewable Energy Sources: Athens, Greece, 2004.
36. UBiPlan. Urban Biometeorology and Planning. Available online: https://ubiplanproject.wordpress.com/ (accessed on 15 March 2026).
37. Lagouvardos, K.; Kotroni, V.; Bezes, A.; Koletsis, I.; Kopania, T.; Lykoudis, S.; Mazarakis, N.; Papagiannaki, K.; Vougioukas, S. The Automatic Weather Stations NOANN Network of the National Observatory of Athens: Operation and Database. *Geosci. Data J.* **2017**, *4*, 4–16. [CrossRef]
38. QGIS Software. QGIS Geographic Information System. *QGIS Association*. Available online: http://www.qgis.org (accessed on 15 March 2026).
39. Stewart, I.D.; Oke, T.R. Local Climate Zones for Urban Temperature Studies. *Bull. Am. Meteorol. Soc.* **2012**, *93*, 1879–1900. [CrossRef]
40. Demuzere, M.; Hankey, S.; Mills, G.; Zhang, W.; Lu, T.; Bechtel, B. Combining Expert and Crowd-Sourced Training Data to Map Urban Form and Functions for the Continental US. *Sci. Data* **2020**, *7*, 264. [CrossRef]
41. Google Earth. Google Earth PRO Athens, Greece. Available online: https://www.google.co.uk/earth/ (accessed on 10 March 2026).
42. ENVI-met. ENVI-Met V4: A Holistic Microclimate Model. Available online: https://envi-met.info/doku.php?id=files:downloadv4 (accessed on 15 March 2026).
43. ENVI-Met. BioMET. Available online: https://envi-met.info/doku.php?id=apps:biomet (accessed on 9 April 2021).
44. Koletsis, I.; Tseliou, A.; Lykoudis, S.; Tsiros, I.; Lagouvardos, K.; Psiloglou, B.; Founda, D.; Pantavou, K. Validation of ENVI-Met Microscale Model with in-Situ Measurements in Warm Thermal Conditions across Athens Area. In *Proceedings of the 17th International Conference on Environmental Science and Technology, Athens, Greece, 1–4 September 2021*; Global NEST (Global Network for Environmental Science and Technology): Athens, Greece, 2021; Volume 17, pp. 1–4.
45. Willmott, C.J. Some Comments on the Evaluation of Model Performance. *Bull.-Am. Meteorol. Soc.* **1982**, *63*, 1309–1313. [CrossRef]
46. Yang, X.; Zhao, L.; Bruse, M.; Meng, Q. Evaluation of a Microclimate Model for Predicting the Thermal Behavior of Different Ground Surfaces. *Build. Environ.* **2013**, *60*, 93–104. [CrossRef]
47. Shinzato, P.; Simon, H.; Silva Duarte, D.H.; Bruse, M. Calibration Process and Parametrization of Tropical Plants Using ENVI-Met V4–Sao Paulo Case Study. *Archit. Sci. Rev.* **2019**, *62*, 112–125. [CrossRef]
48. Salata, F.; Golasi, I.; de Lieto Vollaro, R.; de Lieto Vollaro, A. Outdoor Thermal Comfort in the Mediterranean Area. A Transversal Study in Rome, Italy. *Build. Environ.* **2016**, *96*, 46–61. [CrossRef]
49. Eingrüber, N.; Korres, W.; Löhnert, U.; Schneider, K. Investigation of the ENVI-Met Model Sensitivity to Different Wind Direction Forcing Data in a Heterogeneous Urban Environment. *Adv. Sci. Res.* **2023**, *20*, 65–71. [CrossRef]
50. Stern, P.; Holzer, M.; Kretschmer, F. Implementing Blue-Green Infrastructures in Cities—A Methodological Approach Considering Space Constraints and Microclimatic Benefits. *Sustain. Cities Soc.* **2025**, *126*, 106391. [CrossRef]
51. Middel, A.; Häb, K.; Brazel, A.J.; Martin, C.A.; Guhathakurta, S. Impact of Urban Form and Design on Mid-Afternoon Microclimate in Phoenix Local Climate Zones. *Landsc. Urban Plan.* **2014**, *122*, 16–28. [CrossRef]
52. Stull, R.B. *An Introduction to Boundary Layer Meteorology*; Springer: Dordrecht, The Netherlands, 1988.
53. Bruse, M. ENVI-Met Model Architecture. Available online: https://envi-met.info/doku.php?id=intro:modelconcept#software_versions (accessed on 10 March 2026).

54. Acero, J.A.; Arrizabalaga, J. Evaluating the Performance of ENVI-Met Model in Diurnal Cycles for Different Meteorological Conditions. *Theor. Appl. Climatol.* **2018**, *131*, 455–469. [CrossRef]
55. Liu, Z.; Zheng, S.; Zhao, L. Evaluation of the ENVI-Met Vegetation Model of Four Common Tree Species in a Subtropical Hot-Humid Area. *Atmosphere* **2018**, *9*, 198. [CrossRef]
56. Matzarakis, A.; Rutz, F.; Mayer, H. Modelling Radiation Fluxes in Simple and Complex Environments—Application of the RayMan Model. *Int. J. Biometeorol.* **2007**, *51*, 323–334. [CrossRef]
57. Matzarakis, A.; Rutz, F.; Mayer, H. Modelling Radiation Fluxes in Simple and Complex Environments: Basics of the RayMan Model. *Int. J. Biometeorol.* **2010**, *54*, 131–139. [CrossRef]
58. Pantavou, K.; Santamouris, M.; Asimakopoulos, D.; Theoharatos, G. Empirical Calibration of Thermal Indices in an Urban Outdoor Mediterranean Environment. *Build. Environ.* **2014**, *80*, 283–292. [CrossRef]
59. Venkatramanan, S.; Prasanna, M.V.; Chung, S.Y. *GIS and Geostatistical Techniques for Groundwater Science*; Elsevier: Amsterdam, The Netherlands, 2019.
60. Bowen, G.J.; Revenaugh, J. Interpolating the Isotopic Composition of Modern Meteoric Precipitation. *Water Resour. Res.* **2003**, *39*, 1299. [CrossRef]
61. Bowen, G.J.; Wilkinson, B. Spatial Distribution of Δ18O in Meteoric Precipitation. *Geology* **2002**, *30*, 315–318. [CrossRef]
62. Conrad, O.; Bechtel, B.; Bock, M.; Dietrich, H.; Fischer, E.; Gerlitz, L.; Wehberg, J.; Wichmann, V.; Böhner, J. System for Automated Geoscientific Analyses (SAGA) v. 2.1.4. *Geosci. Model Dev.* **2015**, *8*, 1991–2007. [CrossRef]
63. Sharmin, T.; Steemers, K.; Matzarakis, A. Microclimatic Modelling in Assessing the Impact of Urban Geometry on Urban Thermal Environment. *Sustain. Cities Soc.* **2017**, *34*, 293–308. [CrossRef]
64. Lee, H.; Mayer, H.; Chen, L. Contribution of Trees and Grasslands to the Mitigation of Human Heat Stress in a Residential District of Freiburg, Southwest Germany. *Landsc. Urban Plan.* **2016**, *148*, 37–50. [CrossRef]
65. Acero, J.A.; Herranz-Pascual, K. A Comparison of Thermal Comfort Conditions in Four Urban Spaces by Means of Measurements and Modelling Techniques. *Build. Environ.* **2015**, *93*, 245–257. [CrossRef]
66. Matzarakis, A.; Mayer, H. Another Kind of Environmental Stress: Thermal Stress. *WHO Newsl.* **1996**, *18*, 7–10.
67. Pezzoli, A. Observation and Analysis of Etesian Wind Storms in the Saroniko Gulf. *Adv. Geosci.* **2005**, *2*, 187–194. [CrossRef]
68. Kotroni, V.; Lagouvardos, K.; Lalas, D. The Effect of the Island of Crete on the Etesian Winds over the Aegean Sea. *Q. J. R. Meteorol. Soc.* **2001**, *127*, 1917–1937. [CrossRef]
69. Bartzokas, A.; Metaxas, D.A. Factor Analysis of Some Climatological Elements in Athens, 1931–1992: Covariability and Climatic Change. *Theor. Appl. Climatol.* **1995**, *52*, 195–205. [CrossRef]
70. Koletsis, I.; Lagouvardos, K.; Kotroni, V.; Bartzokas, A. The Interaction of Northern Wind Flow with the Complex Topography of Crete Island-Part 1: Observational Study. *Nat. Hazards Earth Syst. Sci.* **2009**, *9*, 1845–1855. [CrossRef]
71. Elraouf, R.A.; ELMokadem, A.; Megahed, N.; Eleinen, O.A.; Eltarabily, S. Evaluating Urban Outdoor Thermal Comfort: A Validation of ENVI-Met Simulation through Field Measurement. *J. Build. Perform. Simul.* **2022**, *15*, 268–286. [CrossRef]
72. Ouyang, W.; Sinsel, T.; Simon, H.; Morakinyo, T.E.; Liu, H.; Ng, E. Evaluating the Thermal-Radiative Performance of ENVI-Met Model for Green Infrastructure Typologies: Experience from a Subtropical Climate. *Build. Environ.* **2022**, *207*, 108427. [CrossRef]
73. Nastos, P.T.; Moustris, K.P.; Charalampopoulos, I.; Larissi, I.K.; Paliatsos, A.G. Assessment of the Thermal Comfort Conditions in a University Campus Using a 3D Microscale Climate Model, Utilizing Mobile Measurements. In *Perspectives on Atmospheric Sciences*; Springer: Cham, Switzerland, 2017; pp. 309–315.
74. Yang, Y.; Lyu, J.; Du, H.; Lian, Z.; Liu, W.; Duanmu, L.; Zhai, Y.; Cao, B.; Zhang, Y.; Zhou, X.; et al. Main Effects and Interactions of Multiple Key Factors Related to Thermal Perception. *Sci. Total Environ.* **2024**, *918*, 170683. [CrossRef]
75. Liu, S.; Middel, A.; Fang, X.; Wu, R. ENVI-Met Model Performance Evaluation for Courtyard Simulations in Hot-Humid Climates. *Urban Clim.* **2024**, *55*, 101909. [CrossRef]
76. Sinsel, T.; Simon, H.; Ouyang, W.; dos Santos Gusson, C.; Shinzato, P.; Bruse, M. Implementation and Evaluation of Mean Radiant Temperature Schemes in the Microclimate Model ENVI-Met. *Urban Clim.* **2022**, *45*, 101279. [CrossRef]
77. Le, A.-V.; Hip, O.-M.; Yang, S.-Y.; Chan, Y.-C. Sensitivity Analysis of Building Material, Ground Material, and Tree Parameters in Microclimate Simulations. *Urban Clim.* **2024**, *58*, 102184. [CrossRef]
78. Ayyad, Y.N.; Sharples, S. Envi-MET Validation and Sensitivity Analysis Using Field Measurements in a Hot Arid Climate. *IOP Conf. Ser. Earth Environ. Sci.* **2019**, *329*, 12040. [CrossRef]
79. Gregorčič, T.; Ogrin, M.; Repe, B.; Savić, S. Combining Interdisciplinary Field Measurements and ENVI-Met Simulations for Comparative Assessment of Outdoor Human Thermal Comfort across Local Climate Zones. *Sustain. Cities Soc.* **2026**, *142*, 107304. [CrossRef]
80. Zare, S.; Hasheminejad, N.; Shirvan, H.E.; Hemmatjo, R.; Sarebanzadeh, K.; Ahmadi, S. Comparing Universal Thermal Climate Index (UTCI) with Selected Thermal Indices/Environmental Parameters during 12 Months of the Year. *Weather. Clim. Extrem.* **2018**, *19*, 49–57. [CrossRef]

81. Li, J.; Sun, R.; Chen, L. A Review of Thermal Perception and Adaptation Strategies across Global Climate Zones. *Urban Clim.* **2023**, *49*, 101559. [CrossRef]
82. Koutsanitis, S.; Sinou, M.; Kanetaki, Z.; Tousi, E.; Varelidis, G. Thermal Performance Investigation in Historical Urban Neighborhoods Using ENVI-Met Simulation Software. *Land* **2025**, *14*, 284. [CrossRef]
83. Najafian, P.; Hashemi, F.; Khayatian, F.; Van Tran, Q.; López Ochoa, E.; Mehta, S. The ENVI-Met Model for Evaluating Urban Heat Mitigation Strategies in Vulnerable Neighborhoods: A Case Study of San Antonio's Historic Westside. *Urban Clim.* **2026**, *67*, 102893. [CrossRef]